Electronic Supporting Information

for

Dinuclear manganese(III) complexes with bioinspired coordination and variable linkers showing weak exchange effects: a synthetic, structural, spectroscopic and computation study

Sergiu Shova,[a] Angelica Vlad,[a] Maria Cazacu,[a] J. Krzystek,[b] Andrew Ozarowski,[b] Michal Malček, [c]Lukas Bucinsky,[c] Peter Rapta,[c] Joan Cano,[d] Joshua Telser*[e] and Vladimir B. Arion*[f]

[a]Inorganic Polymers Department, "Petru Poni" Institute of Macromolecular Chemistry, Aleea Gr. Ghica Voda 41 A, Iasi 700487, Romania

[b]National High Magnetic Field Laboratory, Florida State University, Tallahassee, Florida 32310, USA

[c]Institute of Physical Chemistry and Chemical Physics, Slovak University of Technology, Radlinského 9, 81237 Bratislava, Slovak Republic

[d]Institut de Ciència Molecular, Universitat de València, Catedrático José Beltrán Martínez 2, 46980 Paterna, Spain

[e]Department of Biological, Physical and Health Sciences, Roosevelt University, 430 S. Michigan Avenue, Chicago, Illinois 60605, USA

[f]Institute of Inorganic Chemistry of the University of Vienna, Währinger Strasse 42, A1090 Vienna, Austria

Table of Contents

Computational details

a) Complexes **1** – **3** contain two Mn^{III} ions that are connected by relatively long bridging ligands; thus, one magnetic Mn^{III} ion was replaced by a non-magnetic Ga^{III} ion in the original crystal structures to determine the axial (*D*) and rhombic (*E*) components of the local (i.e., single-ion) zero-field splitting (ZFS). Theoretical calculations based on an ab initio method, namely the Complete Active Space (CAS) multi-configurational method, on the full $Mn^{III}Ga^{III}$ dinuclear complexes were performed for determining the single-ion ZFS at the DFT level as well, using the PBE functional.[1] These calculations were carried out with version 4.0 of the ORCA programme,[2] using the TZVP basis set proposed by Ahlrichs[3,4] and the auxiliary TZV/C Coulomb fitting basis sets.[5,6,7] The second order contributions to ZFS were evaluated for the five quintet states and 30 triplet excited states generated from an active space with four electrons in five d orbitals. Furthermore, to estimate dynamic electron correlation effects on ZFS parameters, mononuclear models were built by truncation of the original molecules: one of the carboxylate groups of the bridging ligand was replaced by a methyl group; in other words fumarato, terephthalato, and biphenyl-4,4´-dicarboxylato bridges were replaced by but-2-enoato, 4-methylbenzoato, and 4´-methyl-4-biphenylcarboxylato co-ligands, respectively. These calculations were carried out by CAS method and subsequent second-order N-electron valence state perturbation theory (NEVPT2).[8] The *g*-tensors for the spin ground state were calculated using the NEVPT2 method with a first-order perturbation theory on the SOC matrix.[9] The spin−orbit and spin−spin coupling operators in the DFT treatment of ZFS were based on the SOMF scheme.[10] Namely, coupled perturbed (CP), Pederson-Khanna (PK) methods, as well as that based on quasi-restricted orbitals (QRO) were used in the calculation of the spin-orbit contribution of the zero-field splitting.[11]

b) For the sake of comparison with the previous studies on [MnL(NCS] and [MnL(OAc)],[12,13] additional calculations have been performed using the BLYP functional[14] and 6-311G*[15] basis set on single-centre CASSCF and MRCI approaches. All these calculations used the crystal structure geometries of **1** – **3** and were obtained by removing one of the Mn^{III}L moieties and its carboxylate group by a hydrogen atom: fumarato, terephthalato, and biphenyl-4,4´-dicarboxylato bridges were replaced by acrylato, benzoato, and biphenyl-4-carboxylato co-ligands, respectively. In addition, the effect of the solvent molecules present in the crystal

structure has been studied for brevity at the BLYP/6-311G* level (the CP method has been used in the DFT calculations of the spin-orbit contribution of the zero-field splitting). The spin-spin interaction has been accounted for via the Multi-Reference Configuration Interaction (MRCI) approach for the state-averaged quintet CASSCF(4,5) wave function, denoted as MRCI[10,16] throughout the manuscript.

c) In addition, the multi-centre (i.e., both $Mn^{III}L$ moieties and the bridging ligand) CASSCF(8,10) ZFS parameters have been compared to CAS(8,10)-CI results (automatic auxiliary fitting basis set was used). The L-CASCI approach has followed consistently the protocol as described in the literature.[17] The CASCI calculations accounted both for spin-orbit and spin-spin couplings (SOC and SSC, respectively). Note that, the septet {1111011110} determinant was left out of consideration from the total 35 possible determinant due to degeneracy of the lowest septet and nonet states, while all five determinants were taken into account for nonets (taking nonet as the reference state), see the configuration list in Table S5.

Discussion of theoretically determined EPR properties

a) CAS calculations on the $Mn^{III}Ga^{III}$ models, wherein a non-magnetic Ga^{III} ion ($3d^{10}$) replaced a Mn^{III} ion, allowed us to calculate the parameters corresponding to the axial and rhombic components of the local ZFS of **1** – **3**. In all cases, the spin-orbit contribution prevails, with similar contributions from the triplet and quintet excited states (being ca. in a 2:1 ratio, respectively). The positive *D* value is consistent with the axial (tetragonal) compression observed in the three complexes (Table 2), but with a significant rhombic distortion, in agreement with HFEPR spectroscopy. This similar axial distortion in **1** – **3** leads to close *D* values. However, there is a trend that is also corroborated by DFT calculations (Table S2), although this method underestimates the *D* values in manganese(III) complexes, as it has been widely reported in the literature.[13,14,17b] HFEPR of powders or solutions does not provide the orientation of the ZFS. However, this can be calculated and in Fig. S3 are displayed the orientations of the principal axes of the *D* tensors of **1** – **3** in the molecular coordinate system. As expected, the principal *z*-axis (“hard” axis) points at the oxygen atoms of the coordinated phenolato groups, i.e., along the axis of compression. Lastly, the **g**-tensors for **1** – **3** calculated from the NEVPT2 method and ,using an effective Hamiltonian for the spin-orbit coupling (Table S4) agree

moderately with those obtained by HFEPR spectroscopy, with the calculated values being slightly below 2.0 which agrees with the high temperature HFEPR fit in Table 2.
b) CAS calculations in the 6-311G* basis set did not show any significant qualitative deviations from the TZVP ones (see Table 3). The obtained CAS results agree well with each other for the single-centre 6-311G* calculation shown in Table 3. The presence of solvent molecules (see Table S4) in the crystal structures can be considered negligible for the determined BLYP *D* values, see Table S3, and the choice between the particular $Mn^{III}L$ centre has absolutely no effect (not shown). On the contrary, SOC CAS results lead to the increase of *D* parameter with the size of the bridging ligand (see Table 3), while the inclusion of SSC via MRCI reverses this trend in accordance with the experiment (see Table 3). Furthermore, the inclusion of both Mn^{III} centres in BLYP or CAS calculations leads to a considerable underestimation of the *D* parameter (see Table S3), when comparing to the single-centre calculations or experimental results due to ground state degeneracy issues.
c) To improve the assessment of the multicentre approach in a more consistent way with respect to the experiment (or single-centre calculations), the L-CASCI method has been employed (albeit we have to accept that this is a single centre approximation in the multicentre treatment). The L-CASCI rescaled single centre contribution as suggested in Retegan et al.[17a] shows again a very good agreement with the single centre calculations and/or the experimental *D* values. Nevertheless, here taking the SSC contribution into account shows the same trend with the size of the bridging ligands as found for SOC part. For completeness, the calculated **g**-tensor values are also provided in Table S3.

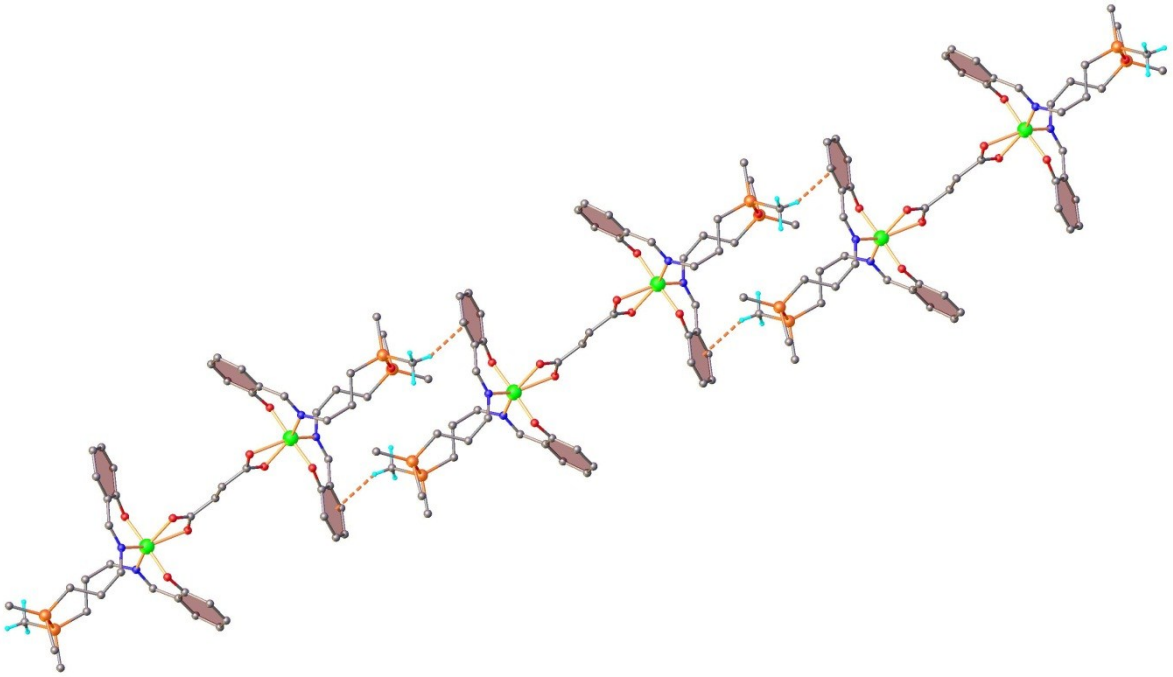

a

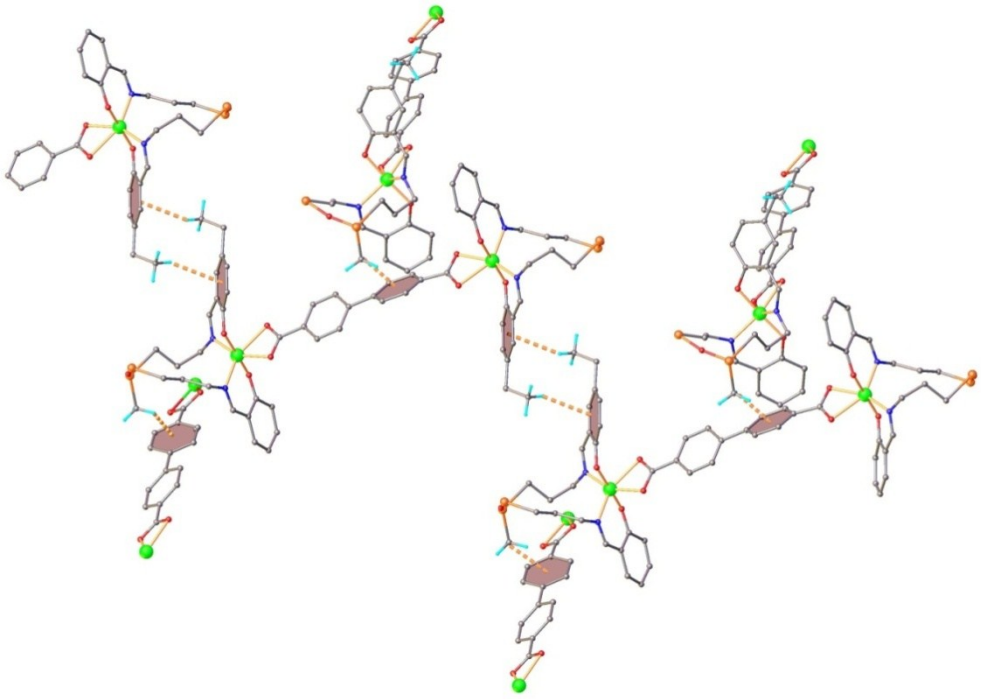

b

Fig. S1. One-dimensional supramolecular chain in the crystal structure of a) **1** and b) **3**. C-H···π distances are shown as dashed orange lines.

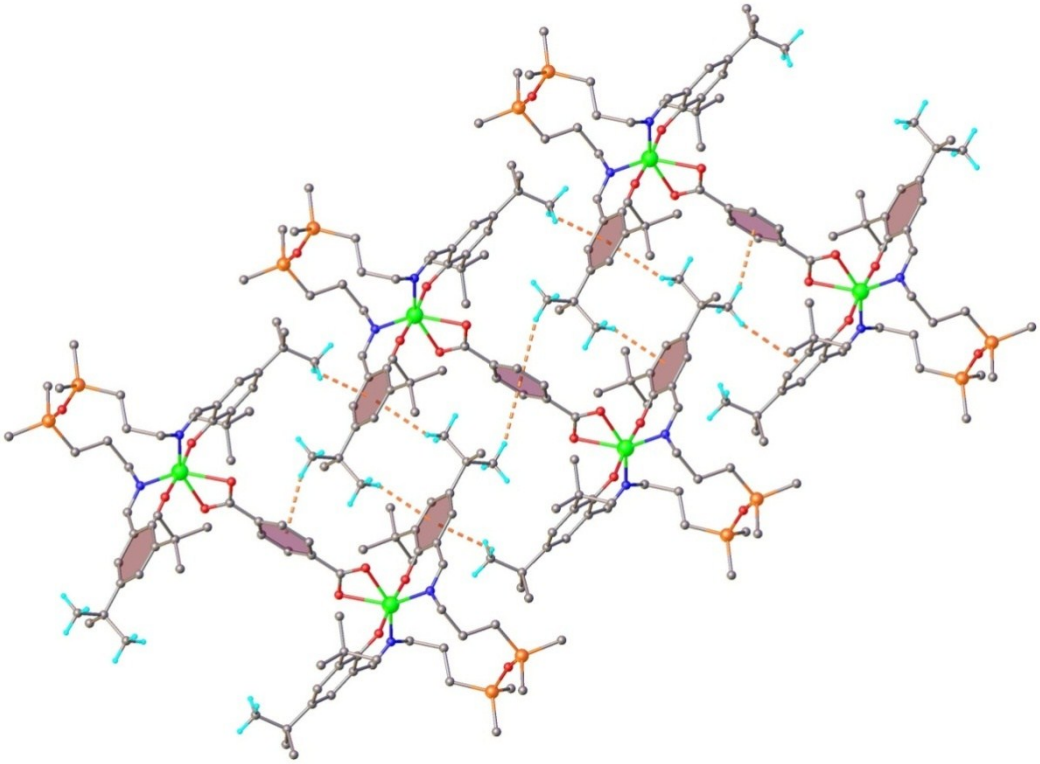

Fig. S2. View of the supramolecular ribbon in the crystal structure **2**. C-H···π distances are shown as dashed orange lines.

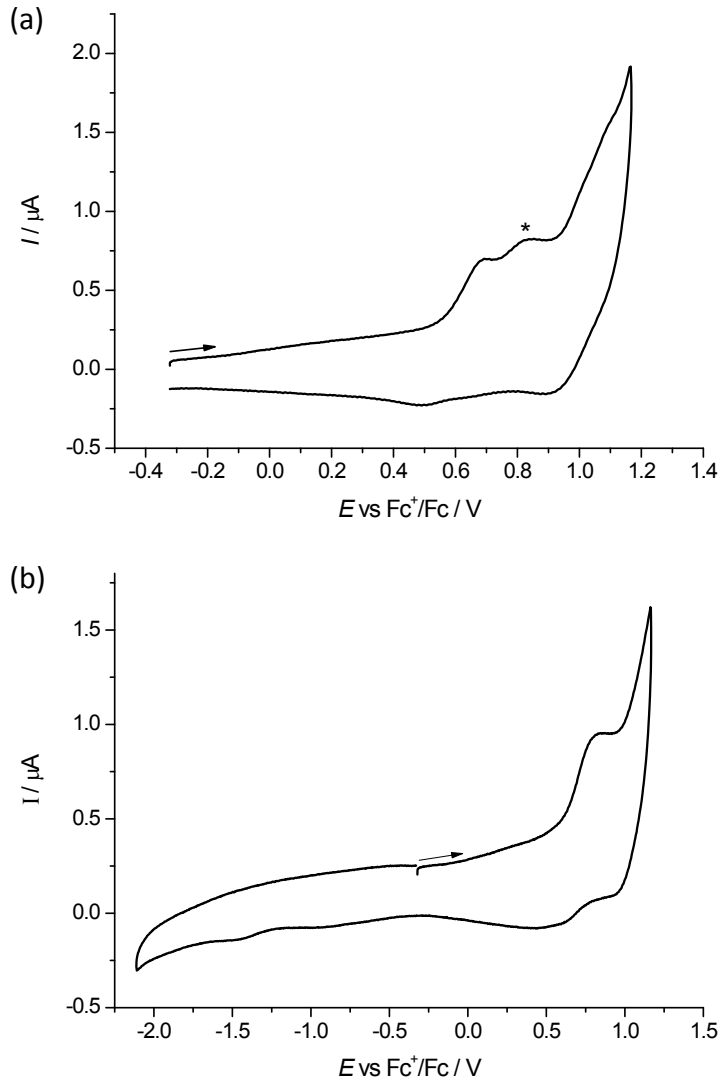

Fig. S3. Cyclic voltammograms in nBu$_4$NPF$_6$/CH$_2$Cl$_2$ of (a) **1**, going to more anodic potentials (asterisk denotes the follow up product) and (b) **2**, going to more anodic potentials and to the cathodic region (GC-disc working electrode, scan rate 100 mV s^{-1}).

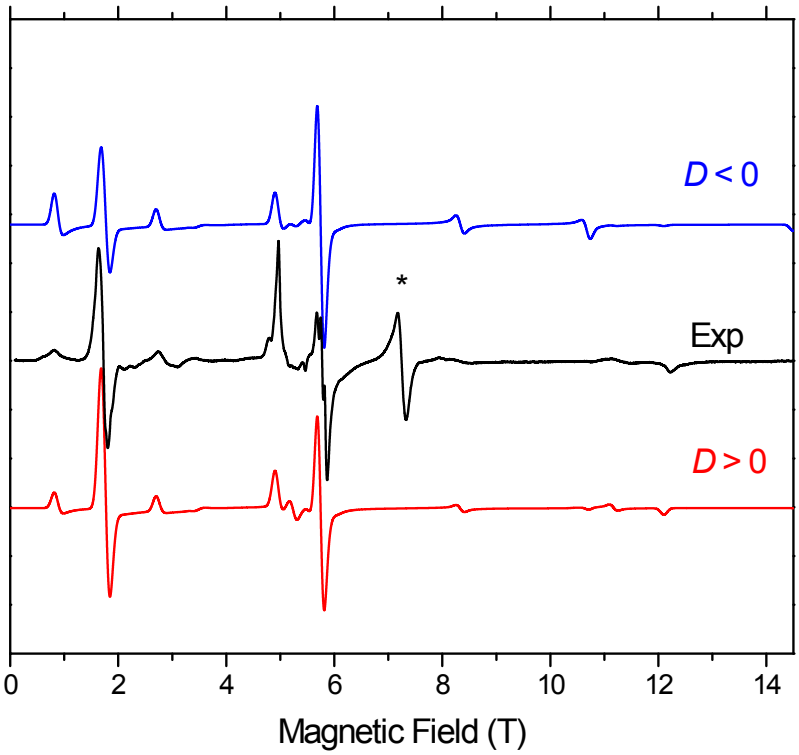

Fig. S4. HFEPR spectra of **1** at 203.2 GHz and 15 K (black trace) accompanied by simulations using spin Hamiltonian parameters as in Table 2. Blue trace: simulations using negative *D*; red trace: positive *D*. The asterisk identifies a signal at $g \approx 2.00$ originating from Mn^{II} that is not simulated.

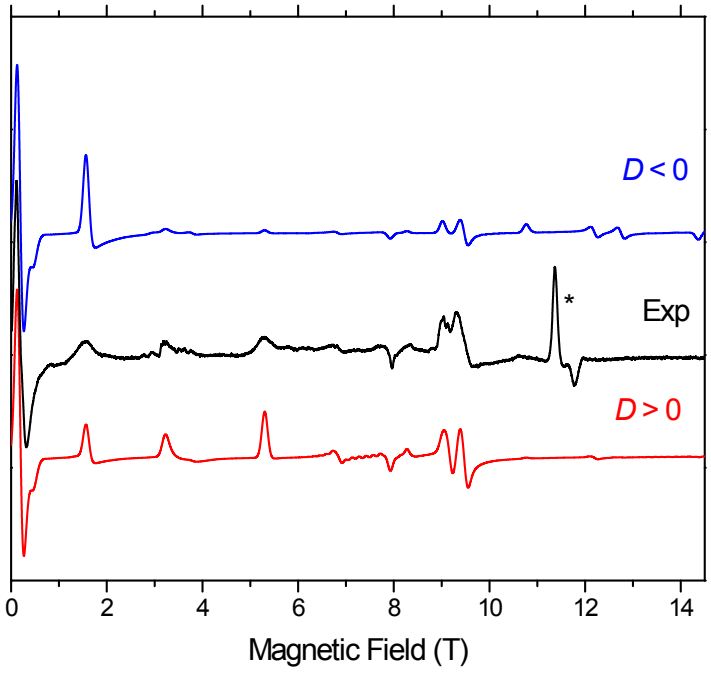

Fig. S5. HFEPR spectra of **1** at 324 GHz (close to one of the zero-field transitions) and 15 K (black trace) accompanied by simulations using spin Hamiltonian parameters as in Table 2. Blue trace: simulations using negative *D*; red trace: positive *D*. The asterisk identifies a signal at $g \approx 2.00$ originating from Mn^{II} that is not simulated.

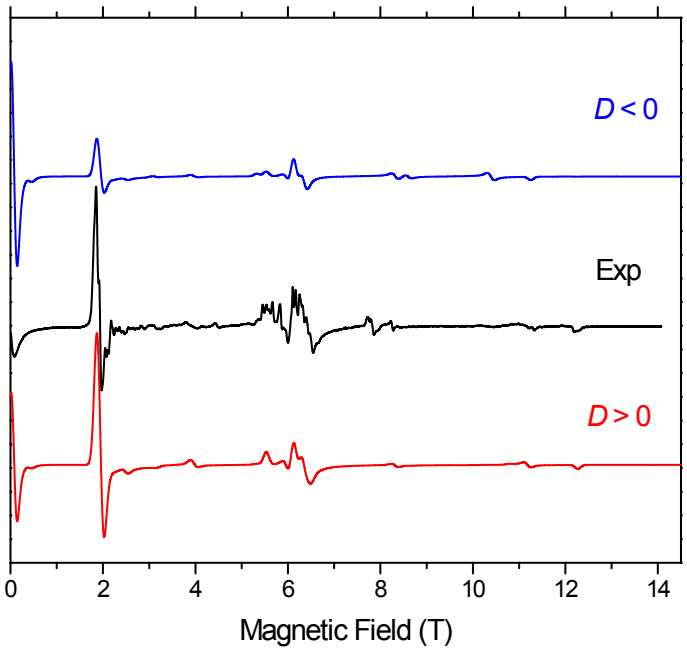

Fig. S6. HFEPR spectra of **2** at 219.2 GHz and 15 K (black trace) accompanied by simulations using spin Hamiltonian parameters as in Table 2. Blue trace: simulations using negative D; red trace: positive D. At this frequency, the near-zero field resonance corresponds to the $3|D - E|$ transition within the $S = 2$ manifold.

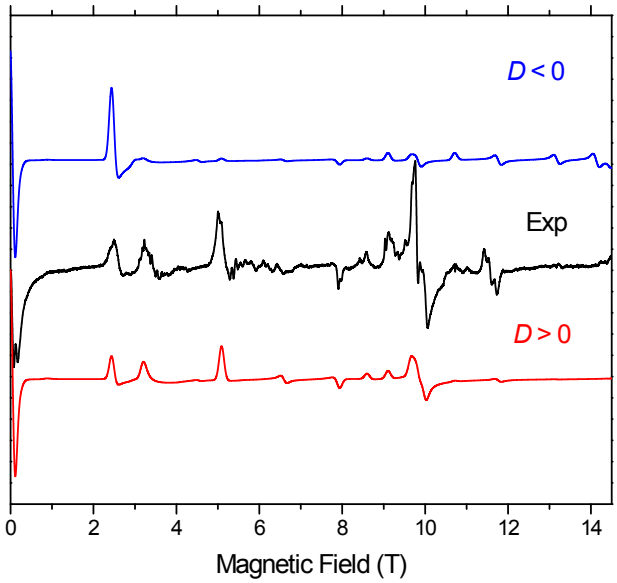

Fig. S7. HFEPR spectra of **2** at 324 GHz and 10 K (black trace, close to one of zero-field transitions) accompanied by simulations using spin Hamiltonian parameters as in Table 1. Blue trace: simulations using negative D; red trace: positive D. At this frequency, the near-zero field resonance corresponds to the $3|D + E| + \Delta$ transition within the $S = 2$ manifold, where $\Delta = 3E^2/D$.

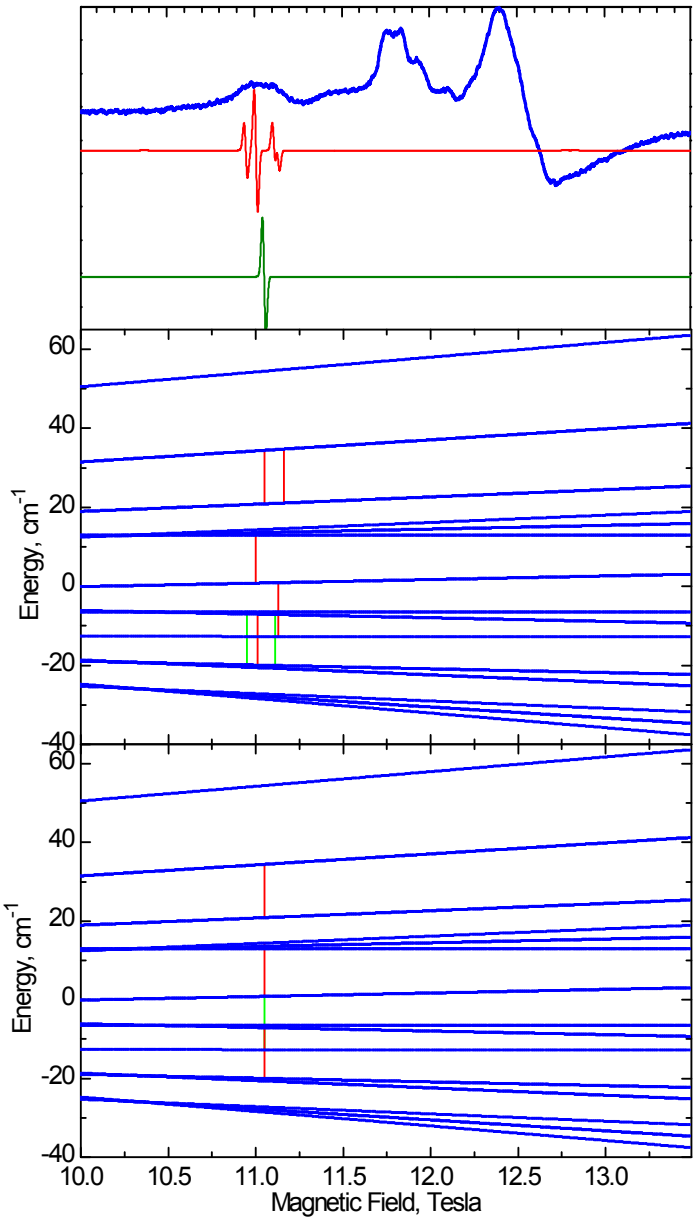

Fig. S8. Top: Fragment of the experimental powder spectrum of **1** (as in Fig. 6, main text; blue trace here) and single-crystal simulations (10 K, 406.4 GHz) using the dimer model with J = –0.025 cm^{-1} (red trace) and "dimer with no interaction" (J = 0; green trace). The latter produces the same EPR simulation as the monomer model. Center and bottom: energy levels of a dimer and "dimer with no interaction", respectively, showing transitions expected at 406.4 GHz. Only transitions with substantial probability are shown. See also Figs. 7 and 9 in main text.

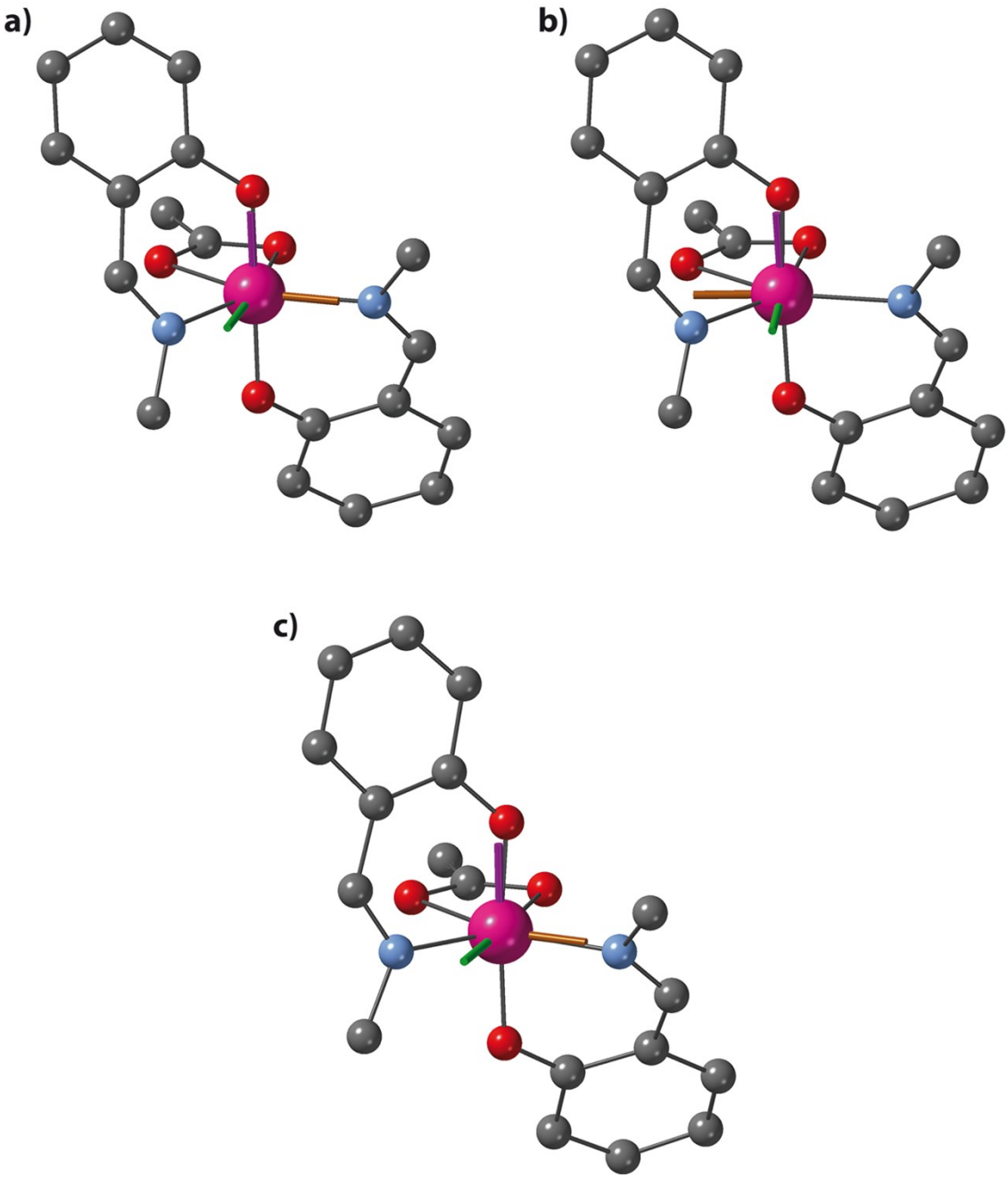

Fig. S9. Relative orientations of the experimental coordination sphere geometry of **1** – **3** (a-c) and the calculated ***D*** tensor (principal directions: *x* = orange, *y* = green, *z* = magenta). Atom colour code: magenta, manganese; blue, nitrogen; red, oxygen; grey, carbon. The calculated D_{zz} direction is nearly aligned with the $O_{(phenolato)}$-Mn-$O_{(phenolato)}$ axis in all cases.

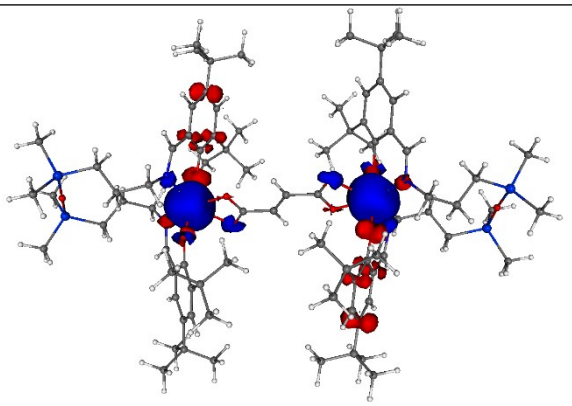

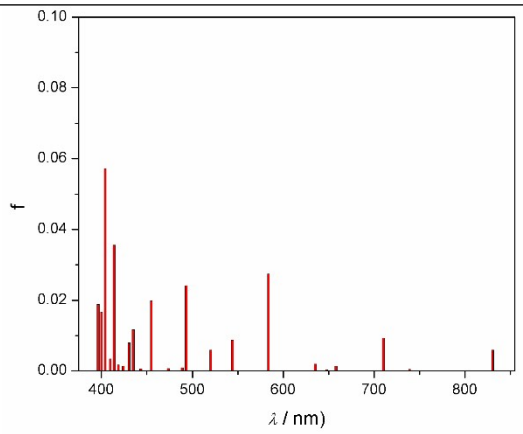

(a) $\mathbf{1}^{+}$ spin(MnL) = 3.458, spin(BL) = 0.085

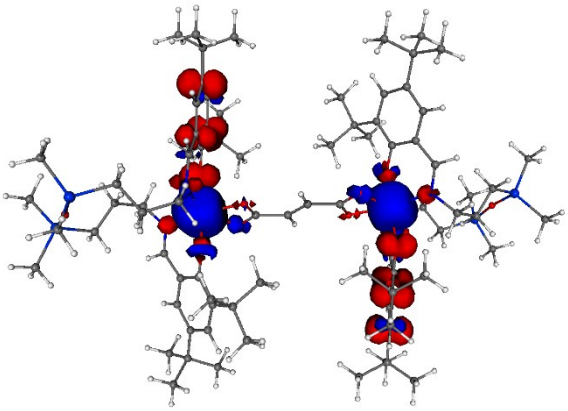

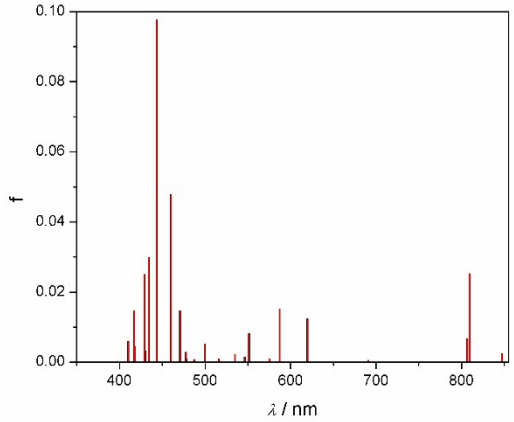

(b) $\mathbf{1}^{2+}$ spin(MnL) = 2.964, spin(BL) = 0.071

Fig. S10. Visualisation of spin density, including spin density populations on each Mn - tetradentate Schiff base moiety MnL and on the bridging ligand BL (left column) and calculated TD-DFT transitions (right column) of $\mathbf{1}^{+}$ (octet) and $\mathbf{1}^{2+}$ (septet) species on (a) and (b), respectively. All the values of spin densities are in a.u. The isovalue was set to ±0.005 a.u.

Table S1. Bond distances (Å) and angles (°) in X-ray crystal structures **1** – **3**.
Compound **1**

Mn1-O1	1.8665(14)	C11-C12	1.536(3)
Mn1-O2	1.8703(14)	C11-C13	1.537(3)
Mn1-O4	2.3420(16)	C11-C14	1.534(3)
Mn1-O5	2.0773(14)	C16-C17	1.530(3)
Mn1-N1	2.0577(16)	C17-C18	1.533(3)
Mn1-N2	2.1301(17)	C23-C24	1.530(3)
Si1-O3	1.6322(16)	C24-C25	1.529(3)
Si1-C18	1.866(2)	C26-C27	1.450(3)
Si1-C19	1.859(3)	C27-C28	1.404(3)
Si1-C20	1.855(2)	C27-C32	1.413(3)
Si2-O3	1.6277(15)	C28-C29	1.372(3)
Si2-C21	1.853(2)	C29-C30	1.405(3)
Si2-C22	1.858(2)	C29-C33	1.533(3)
Si2-C23	1.873(2)	C30-C31	1.390(3)
O1-C1	1.327(2)	C31-C32	1.426(3)
O2-C32	1.331(2)	C31-C37	1.536(3)
O4-C41	1.260(3)	C33-C34	1.536(4)
O5-C41	1.272(3)	C33-C35	1.527(3)
N1-C15	1.288(3)	C33-C36	1.536(4)
N1-C16	1.470(2)	C37-C38	1.539(3)
N2-C25	1.465(2)	C37-C39	1.533(3)
N2-C26	1.287(3)	C37-C40	1.538(3)
C1-C2	1.427(3)	C41-C42	1.478(3)
C1-C6	1.413(3)	C42-C42^{1}	1.328(4)
C2-C3	1.387(3)	Cl1A-C58	1.681(7)
C2-C7	1.531(3)	Cl3-C44	1.682(13)
C3-C4	1.413(3)	Cl3-C58	1.783(5)
C4-C5	1.384(3)	Cl4-C44	1.630(12)
C4-C11	1.529(3)	Cl5-C45	1.720(16)
C5-C6	1.406(3)	Cl6-C45	1.782(16)
C6-C15	1.442(3)	Cl1-C43	1.762(3)
C7-C8	1.536(3)	Cl2-C43	1.749(3)
C7-C9	1.537(3)	Cl7-C46	1.789(6)
C7-C10	1.533(3)	Cl8-C46	1.746(5)

O1-Mn1-O2	177.81(6)	C10-C7-C8	106.93(19)
O1-Mn1-O4	87.63(6)	C10-C7-C9	107.95(18)
O1-Mn1-O5	92.45(6)	C4-C11-C12	110.20(19)
O1-Mn1-N1	88.23(6)	C4-C11-C13	108.83(18)
O1-Mn1-N2	90.76(6)	C4-C11-C14	111.41(19)
O2-Mn1-O4	94.00(6)	C12-C11-C13	109.2(2)
O2-Mn1-O5	89.64(6)	C14-C11-C12	108.4(2)
O2-Mn1-N1	90.26(6)	C14-C11-C13	108.8(2)
O2-Mn1-N2	88.63(6)	N1-C15-C6	126.95(18)
O5-Mn1-O4	59.40(6)	N1-C16-C17	111.26(15)
O5-Mn1-N2	88.83(6)	C16-C17-C18	114.17(16)
N1-Mn1-O4	91.58(6)	C17-C18-Si1	113.48(14)

N1-Mn1-O5	150.89(6)	C24-C23-Si2	115.08(13)
N1-Mn1-N2	120.27(6)	C25-C24-C23	113.80(16)
N2-Mn1-O4	148.05(6)	N2-C25-C24	112.02(15)
O3-Si1-C18	107.90(9)	N2-C26-C27	126.88(18)
O3-Si1-C19	111.00(11)	C28-C27-C26	115.56(17)
O3-Si1-C20	106.82(10)	C28-C27-C32	120.94(18)
C19-Si1-C18	110.19(11)	C32-C27-C26	123.46(18)
C20-Si1-C18	110.46(10)	C29-C28-C27	121.71(19)
C20-Si1-C19	110.39(13)	C28-C29-C30	116.56(19)
O3-Si2-C21	109.84(10)	C28-C29-C33	123.42(19)
O3-Si2-C22	108.27(10)	C30-C29-C33	119.96(19)
O3-Si2-C23	108.45(8)	C31-C30-C29	124.89(19)
C21-Si2-C22	110.17(12)	C30-C31-C32	117.36(18)
C21-Si2-C23	111.07(10)	C30-C31-C37	120.90(18)
C22-Si2-C23	108.97(10)	C32-C31-C37	121.73(17)
C1-O1-Mn1	125.31(12)	O2-C32-C27	121.14(17)
C32-O2-Mn1	125.89(12)	O2-C32-C31	120.31(17)
Si2-O3-Si1	155.64(12)	C27-C32-C31	118.48(17)
C41-O4-Mn1	84.02(12)	C29-C33-C34	108.57(19)
C41-O5-Mn1	95.70(12)	C29-C33-C36	110.53(19)
C15-N1-Mn1	120.19(13)	C34-C33-C36	109.5(2)
C15-N1-C16	117.59(16)	C35-C33-C29	111.71(19)
C16-N1-Mn1	122.06(13)	C35-C33-C34	108.6(2)
C25-N2-Mn1	122.05(13)	C35-C33-C36	107.9(2)
C26-N2-Mn1	119.54(13)	C31-C37-C38	110.19(17)
C26-N2-C25	117.65(16)	C31-C37-C40	112.12(17)
O1-C1-C2	120.79(16)	C39-C37-C31	109.83(16)
O1-C1-C6	120.40(17)	C39-C37-C38	110.15(18)
C6-C1-C2	118.76(17)	C39-C37-C40	107.09(18)
C1-C2-C7	121.32(18)	C40-C37-C38	107.40(18)
C3-C2-C1	117.43(17)	O4-C41-Mn1	66.44(11)
C3-C2-C7	121.24(18)	O4-C41-O5	120.87(18)
C2-C3-C4	124.82(19)	O4-C41-C42	119.5(2)
C3-C4-C11	120.03(19)	O5-C41-Mn1	54.43(10)

C5-C4-C3	116.66(18)	O5-C41-C42	119.60(19)
C5-C4-C11	123.30(18)	C42-C41-Mn1	174.03(17)
C4-C5-C6	121.16(18)	C42[1]-C42-C41	122.0(3)
C1-C6-C15	122.06(18)	C44-Cl3-C58	11.5(6)
C5-C6-C1	121.16(18)	Cl4-C44-Cl3	123.9(11)
C5-C6-C15	116.68(17)	Cl1A-C58-Cl3	113.3(4)
C2-C7-C8	111.47(17)	Cl5-C45-Cl6	116.1(9)
C2-C7-C9	108.70(18)	Cl2-C43-Cl1	111.73(15)
C2-C7-C10	111.98(18)	Cl8-C46-Cl7	113.3(3)
C8-C7-C9	109.7(2)		

Symmetry code: (1) 2 - *x*, 2 - *y*, -*z*.

Compound **2**

Mn1-O2	1.863(4)	C7-C10	1.543(8)
Mn1-O1	1.856(4)	C7-C8	1.538(8)
Mn1-O5	2.152(4)	C7-C9	1.538(8)
Mn1-O4	2.309(4)	C42-C44	1.385(8)
Mn1-N1	2.125(4)	C42-C43	1.389(8)
Mn1-N2	2.089(5)	C4-C3	1.404(8)
Si1-O3	1.625(5)	C4-C5	1.369(8)
Si1-C23	1.865(6)	C4-C11	1.537(7)
Si1-C21	1.859(7)	C27-C26	1.437(8)
Si1-C22	1.858(7)	C27-C32	1.415(8)
Si2-C18	1.867(6)	C27-C28	1.409(8)
Si2-O3	1.633(5)	C44-C43[1]	1.400(8)
Si2-C20	1.886(8)	C17-C16	1.531(7)
Si2-C19	1.852(7)	C29-C30	1.399(9)
Cl2-C45	1.792(10)	C29-C28	1.384(8)
Cl4-C46	1.768(8)	C29-C33	1.528(8)
Cl3-C46	1.765(9)	C31-C30	1.398(8)
O2-C32	1.339(7)	C31-C37	1.526(8)
O1-C1	1.338(7)	C31-C32	1.427(8)
Cl1-C45	1.798(12)	C3-C2	1.385(8)
O5-C41	1.253(7)	C5-C6	1.408(8)
O4-C41	1.267(7)	C37-C38	1.541(8)
N1-C15	1.284(7)	C37-C40	1.542(8)
N1-C16	1.469(7)	C37-C39	1.524(8)
N2-C26	1.288(7)	C13-C11	1.531(9)
N2-C25	1.471(7)	C25-C24	1.528(8)
C15-C6	1.450(8)	C11-C12	1.527(8)
C1-C2	1.425(8)	C11-C14	1.540(9)
C1-C6	1.413(8)	C24-C23	1.528(8)
C41-C42	1.514(7)	C33-C34	1.560(11)
C18-C17	1.530(8)	C33-C35	1.486(10)
C7-C2	1.537(8)	C33-C36	1.517(9)

O2-Mn1-O5	91.91(16)	C44-C42-C43	120.7(5)
O2-Mn1-O4	90.73(15)	C43-C42-C41	120.0(5)
O2-Mn1-N1	91.82(16)	C3-C4-C11	119.1(5)

O2-Mn1-N2	87.38(17)	C5-C4-C3	116.9(5)
O1-Mn1-O2	173.62(16)	C5-C4-C11	124.0(5)
O1-Mn1-O5	94.34(15)	C32-C27-C26	122.4(5)
O1-Mn1-O4	93.62(15)	C28-C27-C26	116.1(5)
O1-Mn1-N1	87.19(16)	C28-C27-C32	121.5(5)
O1-Mn1-N2	87.91(17)	C42-C44-C431	120.1(5)
O5-Mn1-O4	58.82(14)	C18-C17-C16	113.4(5)
N1-Mn1-O5	87.19(16)	C30-C29-C33	120.7(5)
N1-Mn1-O4	145.98(15)	C28-C29-C30	116.3(5)
N2-Mn1-O5	149.35(16)	C28-C29-C33	123.0(6)
N2-Mn1-O4	90.54(16)	C30-C31-C37	121.8(5)
N2-Mn1-N1	123.46(17)	C30-C31-C32	116.6(5)
O3-Si1-C23	108.3(3)	C32-C31-C37	121.6(5)
O3-Si1-C21	108.6(3)	C2-C3-C4	125.2(5)
O3-Si1-C22	109.9(3)	C31-C30-C29	125.9(5)
C21-Si1-C23	109.7(3)	C1-C2-C7	122.2(5)
C22-Si1-C23	110.2(3)	C3-C2-C1	116.9(5)
C22-Si1-C21	110.1(3)	C3-C2-C7	120.9(5)
C18-Si2-C20	112.2(3)	C4-C5-C6	121.2(5)
O3-Si2-C18	107.1(3)	N1-C16-C17	111.1(4)
O3-Si2-C20	108.6(3)	C1-C6-C15	122.2(5)
O3-Si2-C19	108.9(3)	C5-C6-C15	116.8(5)
C19-Si2-C18	110.0(3)	C5-C6-C1	120.8(5)
C19-Si2-C20	109.9(4)	N2-C26-C27	126.7(5)
C32-O2-Mn1	126.7(3)	C31-C37-C38	111.3(5)
C1-O1-Mn1	128.6(3)	C31-C37-C40	112.0(5)
C41-O5-Mn1	93.8(3)	C38-C37-C40	106.8(5)
C41-O4-Mn1	86.2(3)	C39-C37-C31	109.8(5)
C15-N1-Mn1	120.9(4)	C39-C37-C38	110.2(5)
C15-N1-C16	117.4(5)	C39-C37-C40	106.7(5)
C16-N1-Mn1	121.4(3)	O2-C32-C27	120.5(5)
C26-N2-Mn1	120.5(4)	O2-C32-C31	120.9(5)
C26-N2-C25	116.9(5)	C27-C32-C31	118.6(5)
C25-N2-Mn1	122.3(3)	N2-C25-C24	111.0(5)
N1-C15-C6	126.8(5)	C4-C11-C14	108.5(5)
O1-C1-C2	119.7(5)	C13-C11-C4	111.8(5)
O1-C1-C6	121.3(5)	C13-C11-C14	109.0(5)
C6-C1-C2	118.9(5)	C12-C11-C4	110.5(5)
O5-C41-Mn1	57.0(3)	C12-C11-C13	108.3(5)
O5-C41-O4	121.1(5)	C12-C11-C14	108.7(5)
O5-C41-C42	119.3(5)	C23-C24-C25	113.9(5)
O4-C41-Mn1	64.2(3)	C24-C23-Si1	114.1(4)
O4-C41-C42	119.6(5)	C29-C28-C27	121.0(5)
C42-C41-Mn1	175.4(4)	C29-C33-C34	108.0(6)
C17-C18-Si2	114.6(4)	C35-C33-C29	113.8(5)
Si1-O3-Si2	153.8(3)	C35-C33-C34	107.5(6)
C2-C7-C10	111.2(5)	C35-C33-C36	111.5(6)
C2-C7-C8	109.7(5)	C36-C33-C29	109.2(5)
C2-C7-C9	111.5(5)	C36-C33-C34	106.5(6)

C8-C7-C10	107.1(5	C42-C43-C44[1]	119.2(5)
C8-C7-C9	110.3(5)	Cl3-C46-Cl4	111.2(4)
C9-C7-C10	106.9(5)	Cl2-C45-Cl1	108.5(6)
C44-C42-C41	119.3(5)		

Symmetry code: (1) 2 - *x*, 1 - *y*, 1 -*z*.

Compound **3**

Mn1-O1	1.849(3)	C7-C9	1.538(6)
Mn1-O2	1.867(3)	C7-C10	1.529(6)
Mn1-O4	2.256(7)	C11-C12	1.522(7)
Mn1-O5	2.101(9)	C11-C13	1.522(7)
Mn1-N1	2.116(3)	C11-C14	1.539(6)
Mn1-N2	2.077(3)	C16-C17	1.528(6)
Si1-O3	1.591(5)	C17-C18	1.514(6)
Si1-C18	1.885(5)	C23-C24	1.514(7)
Si1-C19	1.82(5)	C24-C25	1.520(5)
Si1-C20	1.892(8)	C26-C27	1.459(5)
Si2-O3	1.611(5)	C27-C28	1.398(6)
Si2-C21	1.864(12)	C27-C32	1.418(5)
Si2-C22	1.821(13)	C28-C29	1.379(6)
Si2-C23	2.062(6)	C29-C30	1.404(6)
O1-C1	1.325(5)	C29-C33	1.535(6)
O2-C32	1.327(5)	C30-C31	1.398(6)
O4-C41	1.265(8)	C31-C32	1.418(6)
O5-C41	1.257(8)	C31-C37	1.539(5)
N1-C15	1.289(5)	C33-C34	1.527(12)
N1-C16	1.455(5)	C33-C35	1.457(12)
N2-C25	1.484(5)	C33-C36	1.507(15)
N2-C26	1.275(5)	C37-C38	1.526(7)
C1-C2	1.426(6)	C37-C39	1.534(6)
C1-C6	1.411(6)	C37-C40	1.533(6)
C2-C3	1.393(6)	C41-C42	1.494(6)
C2-C7	1.525(6)	C44-C45	1.39
C3-C4	1.398(7)	C44-C43	1.39
C4-C5	1.369(6)	C45-C45[1]	1.721(8)
C4-C11	1.550(6)	C45-C46	1.39
C5-C6	1.419(6)	C46-C47	1.39
C6-C15	1.426(6)	C47-C42	1.39
C7-C8	1.544(6)	C42-C43	1.39

O1-Mn1-O2	174.74(12)	C10-C7-C9	107.8(4)
O1-Mn1-O4	94.3(2)	C12-C11-C4	109.8(4)
O1-Mn1-O5	95.2(3)	C12-C11-C14	108.9(4)
O1-Mn1-N1	89.15(12)	C13-C11-C4	111.6(4)
O1-Mn1-N2	88.14(12)	C13-C11-C12	108.8(4)
O2-Mn1-O4	85.2(2)	C13-C11-C14	109.0(4)
O2-Mn1-O5	89.1(3)	C14-C11-C4	108.6(4)
O2-Mn1-N1	93.98(12)	N1-C15-C6	127.6(4)
O2-Mn1-N2	86.67(12)	N1-C16-C17	109.1(3)

O5-Mn1-O4	59.6(2)	C18-C17-C16	113.4(4)
O5-Mn1-N1	88.8(2)	C17-C18-Si1	111.7(3)
N1-Mn1-O4	148.37(18)	C24-C23-Si2	101.6(4)
N2-Mn1-O4	93.91(18)	C23-C24-C25	114.5(4)
N2-Mn1-O5	153.4(2)	N2-C25-C24	110.7(3)
N2-Mn1-N1	117.65(12)	N2-C26-C27	126.4(4)
O3-Si1-C18	110.8(3)	C28-C27-C26	118.0(4)
O3-Si1-C19	107.4(15)	C28-C27-C32	121.1(4)
O3-Si1-C20	105.0(4)	C32-C27-C26	120.8(3)
C18-Si1-C20	106.8(3)	C29-C28-C27	121.9(4)
C19-Si1-C18	110.3(15)	C28-C29-C30	116.2(4)
C19-Si1-C20	116.5(14)	C28-C29-C33	121.7(4)
O3-Si2-C21	110.8(5)	C30-C29-C33	122.1(4)
O3-Si2-C22	107.4(5)	C31-C30-C29	124.7(4)
O3-Si2-C23	106.4(3)	C30-C31-C32	117.7(4)
C21-Si2-C23	115.1(4)	C30-C31-C37	121.6(4)
C22-Si2-C21	108.8(6)	C32-C31-C37	120.7(3)
C22-Si2-C23	108.0(5)	O2-C32-C27	120.7(3)
C1-O1-Mn1	131.8(2)	O2-C32-C31	121.2(3)
C32-O2-Mn1	122.3(2)	C27-C32-C31	118.1(3)
Si1-O3-Si2	166.8(4)	C34-C33-C29	110.0(5)
C15-N1-Mn1	121.6(3)	C35-C33-C29	110.5(5)
C15-N1-C16	117.9(3)	C35-C33-C34	113.7(9)
C16-N1-Mn1	120.3(3)	C35-C33-C36	111.2(10)
C25-N2-Mn1	124.1(2)	C36-C33-C29	105.2(7)
C26-N2-Mn1	118.1(3)	C36-C33-C34	105.8(10)
C26-N2-C25	117.6(3)	C38-C37-C31	108.8(3)
O1-C1-C2	118.7(4)	C38-C37-C39	108.2(4)
O1-C1-C6	121.7(4)	C38-C37-C40	110.7(4)
C6-C1-C2	119.6(4)	C39-C37-C31	112.1(4)
C1-C2-C7	121.0(4)	C40-C37-C31	110.4(3)
C3-C2-C1	116.8(4)	C40-C37-C39	106.6(4)
C3-C2-C7	122.1(4)	O4-C41-C42	120.5(7)
C2-C3-C4	124.9(4)	O5-C41-O4	118.6(7)
C3-C4-C11	120.1(4)	O5-C41-C42	120.8(7)
C5-C4-C3	117.1(4)	C45-C44-C43	120
C5-C4-C11	122.7(4)	C44-C45-C45[1]	127.1(6)
C4-C5-C6	121.8(4)	C44-C45-C46	120
C1-C6-C5	119.7(4)	C46-C45-C45[1]	104.1(6)
C1-C6-C15	123.5(4)	C45-C46-C47	120
C5-C6-C15	116.8(4)	C42-C47-C46	120
C2-C7-C8	111.6(3)	C47-C42-C41	120.4(4)
C2-C7-C9	109.3(3)	C47-C42-C43	120
C2-C7-C10	111.8(4)	C43-C42-C41	119.6(4)
C9-C7-C8	108.9(4)	C42-C43-C44	120
C10-C7-C8	107.4(4)		

Symmetry code: (1) 1 - *x*, 2 - *y*, -*z*.

Table S2. Calculated values of D (in cm^{-1}) and E/D (in parentheses) for **1** – **3** from the coupled perturbed (CP), Pederson-Khanna (PK) methods, as well as that based on quasi-restricted orbitals (QRO) applied on the wavefunctions obtained with the PBE functional.

Compound	PK	CP	QRO
1	+1.45 (0.236)	+1.74 (0.231)	+2.32 (0.230)
2	+1.48 (0.149)	+1.77 (0.143)	+2.40 (0.139)
3	+1.60 (0.142)	+1.92 (0.139)	+2.50 (0.145)

Table S3. Calculated values of the *D* (in cm^{-1}), *E*/*D* ratio, and ***g***-tensor components of **1** – **3** species obtained at the different levels of theory (6-311G* basis set). Herein, "single" means that only one Mn^{III} centre has been taken into account (terminated geometry) and "solv" indicates that system contains also solvent molecules from the crystal structure.

System	Method	*D*	*E*/*D*	g_{xx}	g_{yy}	g_{zz}	g_{iso}
1-single	BLYP	1.542	0.242	1.996	2.000	2.004	2.000
1-single	CAS	2.941	0.228	1.970	1.982	1.998	1.983
1-single	MRCI	3.637	0.136				
1-single+solv.	BLYP	1.545	0.235	1.996	2.000	2.004	2.000
1	BLYP	0.750	0.242	1.996	2.000	2.004	2.000
1	CAS	0.521	0.251	1.973	1.983	1.999	1.985
1	L-CASCI (SOC)	1.528	0.207				
1	L-CASCI (SOC+SSC)	1.709	0.212				
1+solv.	BLYP	0.751	0.238	1.997	2.000	2.004	2.000
2-single	BLYP	1.587	0.140	1.997	1.999	2.004	2.000
2-single	CAS	3.034	0.154	1.971	1.979	1.999	1.983
2-single	MRCI	3.522	0.159				
2-single+solv.	BLYP	1.580	0.138	1.997	1.999	2.004	2.000
2	BLYP	0.772	0.139	1.997	1.999	2.004	2.000
2	CAS	0.547	0.162	1.974	1.981	1.999	1.985
2	L-CASCI (SOC)	1.590	0.138				
2	L-CASCI (SOC+SSC)	1.771	0.144				
2+solv.	BLYP	0.769	0.138	1.997	1.999	2.004	2.000
3-single	BLYP	1.680	0.128	1.997	1.999	2.004	2.000
3-single	CAS	3.144	0.133	1.971	1.979	1.999	1.983
3-single	MRCI	3.413	0.232				
3-single+solv.	BLYP	1.670	0.128	1.997	1.999	2.004	2.000
3	BLYP	0.818	0.128	1.997	1.999	2.004	2.000
3	CAS	0.555	0.156	1.974	1.981	1.999	1.985
3	L-CASCI (SOC)	1.645	0.120				
3	L-CASCI (SOC+SSC)	1.834	0.124				
3+solv.	BLYP	0.814	0.128	1.997	1.999	2.004	2.000

Table S4. Calculated ***g***-tensor components through NEVPT2 results for **1** – **3**.

Compound	g_x	g_y	g_z	g_{iso}
1	1.975	1.985	1.999	1.986
2	1.976	1.982	1.999	1.986
3	1.976	1.983	1.999	1.986

Table S5. L-CASCI reference space used in model (c). Note that, the septet {1111011110} determinant was left out of consideration. (Note that the first five d-orbitals are localised on the Mn1 centre and the other five on the Mn2 centre.)

Nonets:
{ 1 1 1 1 0 1 1 1 1 0 }
{ 1 1 1 1 0 1 1 1 0 1 }
{ 1 1 1 1 0 1 1 0 1 1 }
{ 1 1 1 1 0 1 0 1 1 1 }
{ 1 1 1 1 0 0 1 1 1 1 }
Septets:
{ 1 1 1 1 0 1 1 1 0 1 }
{ 1 1 1 1 0 1 1 0 1 1 }
{ 1 1 1 1 0 1 0 1 1 1 }
{ 1 1 1 1 0 0 1 1 1 1 }
{ 1 1 1 1 0 2 1 1 0 0 }
{ 1 1 1 1 0 2 1 0 1 0 }
{ 1 1 1 1 0 2 1 0 0 1 }
{ 1 1 1 1 0 2 0 1 1 0 }
{ 1 1 1 1 0 2 0 1 0 1 }
{ 1 1 1 1 0 2 0 0 1 1 }
{ 1 1 1 1 0 1 2 1 0 0 }
{ 1 1 1 1 0 1 2 0 1 0 }
{ 1 1 1 1 0 1 2 0 0 1 }
{ 1 1 1 1 0 0 2 1 1 0 }
{ 1 1 1 1 0 0 2 1 0 1 }
{ 1 1 1 1 0 0 2 0 1 1 }
{ 1 1 1 1 0 1 1 2 0 0 }
{ 1 1 1 1 0 1 0 2 1 0 }
{ 1 1 1 1 0 1 0 2 0 1 }
{ 1 1 1 1 0 0 1 2 1 0 }
{ 1 1 1 1 0 0 1 2 0 1 }
{ 1 1 1 1 0 0 0 2 1 1 }
{ 1 1 1 1 0 1 1 0 2 0 }
{ 1 1 1 1 0 1 0 1 2 0 }
{ 1 1 1 1 0 1 0 0 2 1 }
{ 1 1 1 1 0 0 1 1 2 0 }
{ 1 1 1 1 0 0 1 0 2 1 }
{ 1 1 1 1 0 0 0 1 2 1 }
{ 1 1 1 1 0 1 1 0 0 2 }
{ 1 1 1 1 0 1 0 1 0 2 }
{ 1 1 1 1 0 1 0 0 1 2 }
{ 1 1 1 1 0 0 1 1 0 2 }
{ 1 1 1 1 0 0 1 0 1 2 }
{ 1 1 1 1 0 0 0 1 1 2 }

References

1. (a) J. P. Perdew, K. Burke, M. Ernzerhof, M. *Phys. Rev. Lett.*1997, **78**, 1396; (b) J. P. Perdew, K. Burke, M. Ernzerhof, *Phys. Rev. Lett.*1996, **77**, 3865–3868.
2. F. Neese, Wiley Interdiscip. Rev. Comput. Mol. Sci. 2018, **8**, e1327.
3. A. Schäfer, C. Huber, R. Ahlrichs, *J. Chem. Phys.*1994, **100**, 5829–5835.
4. A. Schäfer, H. Horn, R. Ahlrichs, *J. Chem. Phys.*1992, **97**, 2571–2577.
5. K. Eichkorn, O. Treutler, H. Ohm, M. Haser, R. Ahlrichs, *Chem. Phys. Lett.*1995, **240**, 283–290.
6. K. Eichkorn, O. Treutler, H. Ohm, M. Haser, R. Ahlrichs, *Chem. Phys. Lett.*1995, **242**, 652–660.
7. K. Eichkorn, O. Treutler, H. Ohm, M. Haser, R. Ahlrichs, *Theor. Chem. Acc.*1997, **97**, 119–124.
8. (a) C. Angeli, R. Cimiraglia, S. Evangelisti, T. Leininger, J.-P. Malrieu, *J. Chem. Phys*. 2001, **114**,10252; (b) C. G. Werncke, E. Suturina, P. C. Bunting, L. Vendier, J. R. Long, M. Atanasov, M.; Neese, F.; Sabo-Etienne, S.; Bontemps, *Chem. Eur. J*. 2016, **22**, 1668-1674.
9. S. Vancoillie, J. Chalupský, U. Ryde, E. I. Solomon, K. Pierloot, F. Neese, L. Rulíšek. *J. Phys. Chem. B*2010, **114**, 7692–7702.
10. F. Neese, *J. Am. Chem. Soc.* 2006, **128**, 10213–10222.
11. F. Neese, *J. Chem. Phys.* 2007, **127**, 164112.
12. M. Cazacu, S. Shova, A. Soroceanu, P. Machata, L. Bucinsky, M. Breza, P. Rapta, J. Telser, J. Krzystek, V. B. Arion, *Inorg. Chem.*, 2015, **54**, 5691–5706.
13. S. Shova, A. Vlad, M. Cazacu, J. Krzystek, L. Bucinsky, M. Breza, D. Darvasiová, P. Rapta, J. Cano, J. Telser, V. B. Arion, *Dalton Trans.*, 2017, **46**, 11817–11829.
14. (a) A. D. Becke, *Phys Rev A*. 1988, **38**, 3098; (b) C. Lee, W. Yang, R. G. Parr, Phys Rev B. 1988, **37**, 785.
15. (a) R. Krishnan, J. S. Binkley, R. Seeger, J. A. Pople, *J. Chem. Phys*. 1980, **72**, 650; (b) A. D. McLean, G. S. Chandler, J. Chem. Phys. 1980, **72**, 5639.
16. C. Duboc, D. Ganyushin, K. Sivalingam, M. N. Collomb, F. Neese, *J. Phys. Chem*. A, 2010, **114**, 10750−10758.
17. (a) M. Retegan, N. Cox, D. A. Pantazis, and F. Neese, Inorg. Chem. 2014, **53**, 11785–11793; (b) H. Fliegl, K. Fink, W. Klopper, C. E. Anson, A. K. Powell, R.

Clérac, *Phys. Chem. Chem. Phys*. 2009, **11**, 3900–3909.